PROCEEDINGS, TOUGH Symposium 2003
Lawrence Berkeley National Laboratory, Berkeley, California, May 12–14, 2003

MODELING SUPERCRITICAL CO_2 INJECTION IN HETEROGENEOUS POROUS MEDIA

Christine Doughty and Karsten Pruess

Earth Sciences Division
E.O. Lawrence Berkeley National Laboratory
Berkeley, CA, 94720, U.S.A.
e-mail: cadoughty@lbl.gov

ABSTRACT

We investigate the physical processes that occur during the sequestration of CO_2 in brine-bearing geologic formations using TOUGH2. An equation of state package that treats a two-phase (liquid, gas), three-component (water, salt, and CO_2) system is employed. CO_2 is injected in a supercritical state that has a much lower density and viscosity than the liquid brine it displaces. In situ, the supercritical CO_2 forms a gas-like phase, and also partially dissolves in the aqueous phase. Chemical reactions between CO_2 and rock minerals that could potentially contribute to mineral trapping of CO_2 are not included. The geological setting considered is a fluvial/deltaic formation that is strongly heterogeneous, making preferential flow a significant effect, especially when coupled with the strong buoyancy forces acting on the gas-like CO_2 plume. Key model development concerns include vertical and lateral grid resolution, grid orientation effects, and the choice of characteristic curves

INTRODUCTION

The risks associated with increased concentrations of greenhouse gases in the atmosphere have prompted study of the feasibility of geological sequestration of carbon dioxide (CO_2) produced by power plants, refineries, and other industrial concerns that produce localized sources of CO_2. We investigate the physical processes that occur during the sequestration of CO_2 in brine-bearing geologic formations. Other potential sites for sequestration include coal beds and depleted oil and gas reservoirs. Among the motivations for using brine formations are their widespread availability and lack of competing uses. Brine formations associated with oil reservoirs often have the added advantages of being well characterized and in close proximity to CO_2 sources.

Several other recent studies (van der Meer, 1995; Pruess and Garcia, 2002; Pruess et al., 2003) have also investigated CO_2 sequestration in brine formations, but they have all employed rather idealized representations of the geology. The present paper is part of an on-going effort to investigate the impact of heterogeneity on the capacity of the subsurface to sequester CO_2 (Doughty et al., 2001; Doughty et al., 2002; Knox et al., 2003).

FLOW AND TRANSPORT PROCESSES

We employ TOUGH2 (Pruess et al., 1999) with the equation of state package ECO2, which treats a two-phase (liquid, gas), three-component (water, salt, and CO_2) system in the pressure/temperature regime above the critical point of CO_2 (P = 73.8 bars, T = 31°C). ECO2 was adapted from EWASG (Battistelli et al., 1997), which treats the same components under sub-critical point conditions, and was designed for geothermal reservoir simulation. Supercritical CO_2 properties were taken from Altunin (1975), as implemented by Malkovsky (private communication, 1999). Although ECO2 may include temperature variations, we use it in isothermal mode here.

CO_2 is injected in a supercritical state that has a much lower density and viscosity than the liquid brine it displaces. In situ, the supercritical CO_2 partitions between an immiscible gas-like phase and dissolution in the aqueous phase, according to an extended version of Henry's Law. The present simulations are relatively short-term (less than 60 years), so they emphasize advective processes. Slower flow processes such as aqueous-phase diffusion of dissolved species and the buoyancy effect of dissolved CO_2 are not included. Salt may precipitate out of the brine, but the rock matrix itself is inert. Thus, chemical reactions between CO_2 and rock minerals that could potentially contribute to mineral trapping of CO_2 are not considered.

GEOLOGICAL SETTING AND MODEL DEVELOPMENT

The geological setting for our model is the fluvial/deltaic Frio formation in the upper Texas gulf coast (Galloway, 1982; Hovorka et al., 2001). We construct 3D models stochastically, with model layers derived from idealized representations of fluvial depositional settings including barrier bars (continuous very high-permeability sands), distributary channels (intermingled sands and shales, with a large high-permeability sand component), and shaley layers (predominantly low-permeability

discontinuous shale lenses, interspersed with moderate-permeability sand), as shown in Figure 1. The program TproGS (Carle and Fogg, 1996, 1997; Fogg et al., 2001) constructs stochastic representations of individual layers consistent with the idealized representations. Each layer contains three material types, and the vertical sequence of layers is determined by analysis of well logs. Overall, permeability varies by nearly six orders of magnitude among material types, making preferential flow a significant effect, especially when coupled with the strong buoyancy forces acting on the gas-like CO_2 plume.

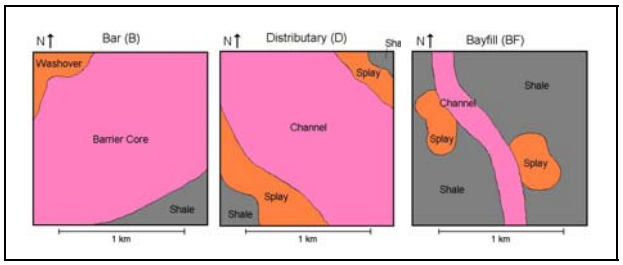

Figure 1. Idealized representations of fluvial depositional settings used by TproGS to generate stochastic permeability fields.

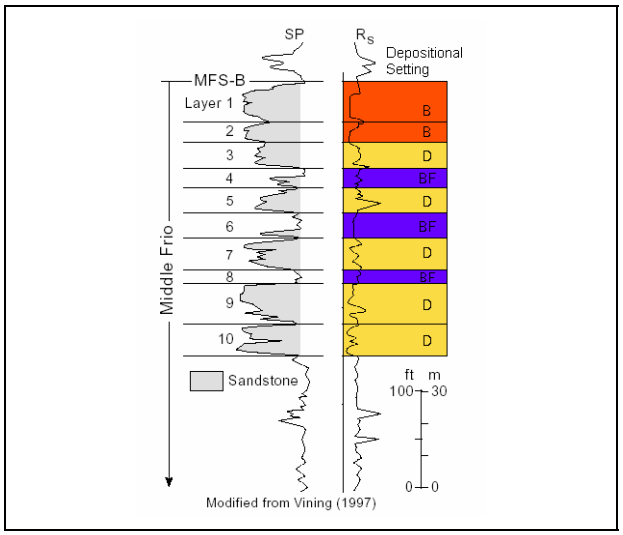

Figure 2. Well logs and interpretation of sequence of depositional settings for Umbrella Point model.

Two TOUGH2 models have been developed. The first, the Umbrella Point model, is based on the well logs shown in Figure 2. The model (Figure 3), is 1 km by 1 km by 100 m thick, and is intended to represent the scale on which CO_2 from a single power plant might be stored. The model is bounded above and below by closed boundaries, which represent continuous shale layers. Lateral boundaries are open (constant-pressure), to represent natural spill points of sequestration regions. Within the model, several discontinuous shaley layers exist that strongly retard flow. Table 1 summarizes the material properties used in the model. Due to a lack of data on two-phase flow properties of supercritical CO_2 and liquid brines, generic characteristic curves are used: van Genuchten (1980) for liquid relative permeability and capillary pressure and Corey (1954) for gas relative permeability.

As in most 3D model applications, we must balance the need for adequate spatial resolution with a computationally manageable number of grid blocks. Grid-block thicknesses vary with depth to resolve geologic layering, while the lateral grid spacing is uniform. In our basic grid, one model layer represents each of the ten depositional layers. Alternative grids that provide two or three model layers per depositional layer have also been developed.

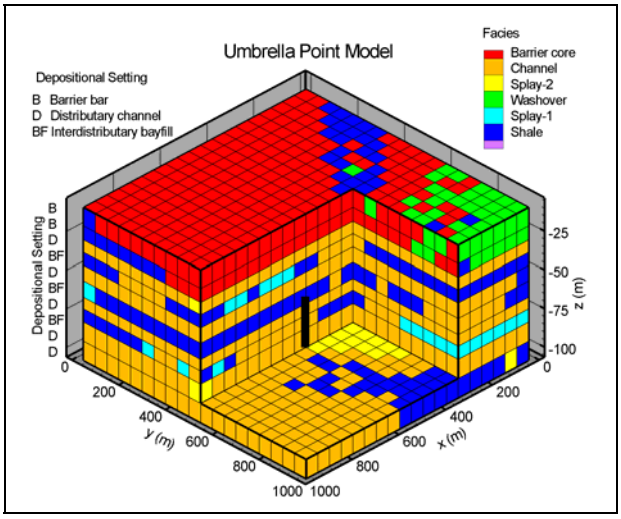

Figure 3. Cut-away view of Umbrella Point model.

Table 1. Material properties for Umbrella Point model. For each depositional setting, framework facies is shown in bold.

Depositional Setting	Material	Permeability (md)	Porosity (%)
Barrier bar (B)	**Barrier core**	**700**	**32**
	Washover	200	29
	Shale	0.001	10
Distributary channel (D)	**Channel**	**400**	**30**
	Splay-2	250	30
	Shale	0.001	10
Interdistributary bayfill (BF)	Channel	400	30
	Splay-1	150	28
	Shale	**0.001**	**10**

The second model (Figure 4) is 440 m by 440 m by 12 m thick, and represents the site of an upcoming pilot test of CO_2 sequestration in the Frio formation at the South Liberty field near Houston, Texas. As in the first model, closed upper and lower boundaries represent continuous shale layers, but in this model, three of the four lateral boundaries are also closed to represent the edges of a fault block. The model includes three depositional settings, each composed of multiple grid layers. In the deepest depositional setting, an upward-coarsening sand, permeability varies with depth as well as facies. Table 2 summarizes the material properties used in the model. Our basic South Liberty model uses the same generic characteristic curves as the Umbrella Point model, but characteristic curves believed to be more representative of local conditions have also been employed.

In this pilot-scale model, vertical grid spacing varies to represent geology. Lateral grid spacing is also variable, with finer resolution around injection and monitoring well locations. Unlike the Umbrella Point model, which has horizontal layers, here layers dip at 15 degrees, with the open end of the model in the down-dip direction. Hence, buoyancy flow plays two important roles, moving CO_2 to the top of the formation and also up-dip toward the closed end of the fault block. The combination of these buoyancy-driven movements and the radial flow away from the injection well provides a challenge for a rectangular grid. Our basic model uses five-point differencing, but an alternative model using nine-point differencing for lateral connections has also been developed.

Table 2. Material properties for South Liberty model. For each depositional setting, framework facies is shown in bold.

Depositional Setting	Material	Permeability (md) k_h	Permeability (md) k_v	Porosity (%)
Distributary channel (D)	**Channel-2**	**286**	**114**	**28**
	Splay-2	78	31	21
	Shale	0.12	0.012	5
Thin shale layer (BF)	Channel-1	63	16	20
	Splay-1	17	4	15
	Shale	**0.12**	**0.012**	**5**
Upward-coarsening sand (B)	**Barrier core**	**63-286**	**16-191**	**20-28**
	Washover	17-78	4-52	15-21
	Shale	0.12	0.012	5

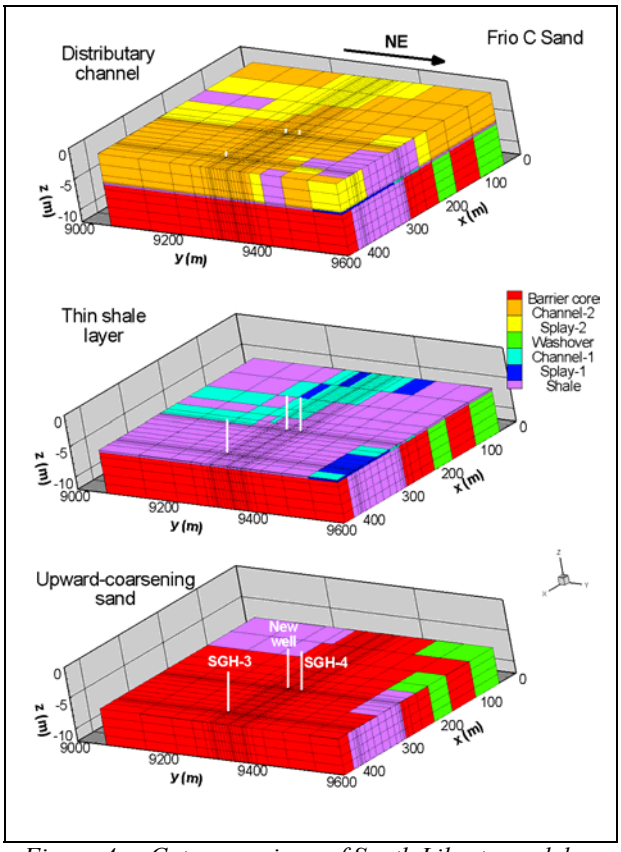

Figure 4a. Cut-away views of South Liberty model.

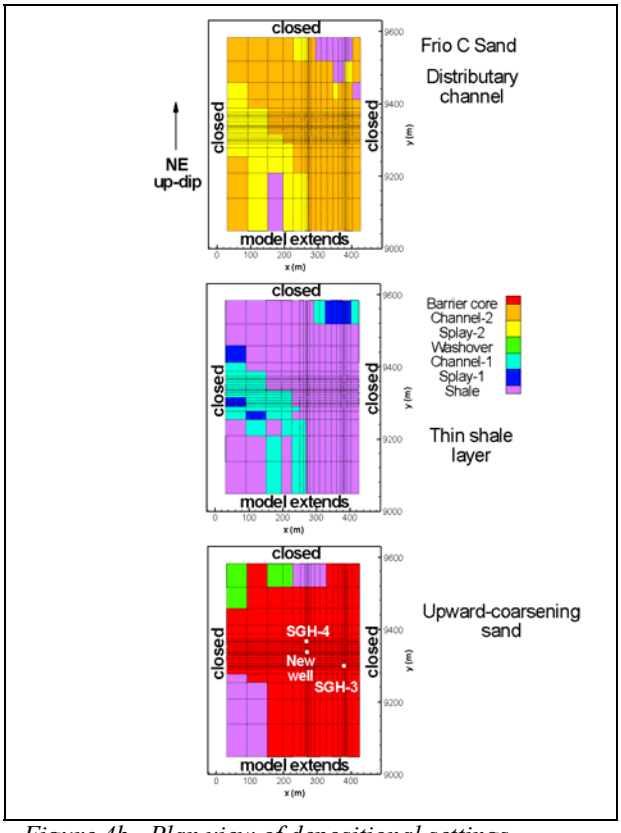

Figure 4b. Plan view of depositional settings.

SIMULATION RESULTS

For both models, we begin with single-phase liquid brine under hydrostatic, isothermal conditions, and inject supercritical CO_2 through a single injection well screened over the lower half of the model.

Umbrella Point Power Plant Model

CO_2 is injected at a rate of 680,000 metric tons per year (21.6 kg/s) for a period of 20 years, then the system is monitored for an additional 80 years to watch the evolution of the CO_2 plume. This injection rate represents about half of the CO_2 output from a 1,000 MW gas-fired power plant. Initial formation conditions are P = 188 bars, T = 78°C, and TDS = 100,000 ppm. Under these conditions, CO_2 has a density of 577 kg/m^3 and a viscosity of $4.4 \cdot 10^{-5}$ Pa·s.

Figure 5 shows a time sequence of spatial distributions of CO_2 in the immiscible gas-like phase during the injection period. Strongly preferential flow occurs, as buoyant CO_2 finds gaps in the shale layers and moves into the upper half of the model.

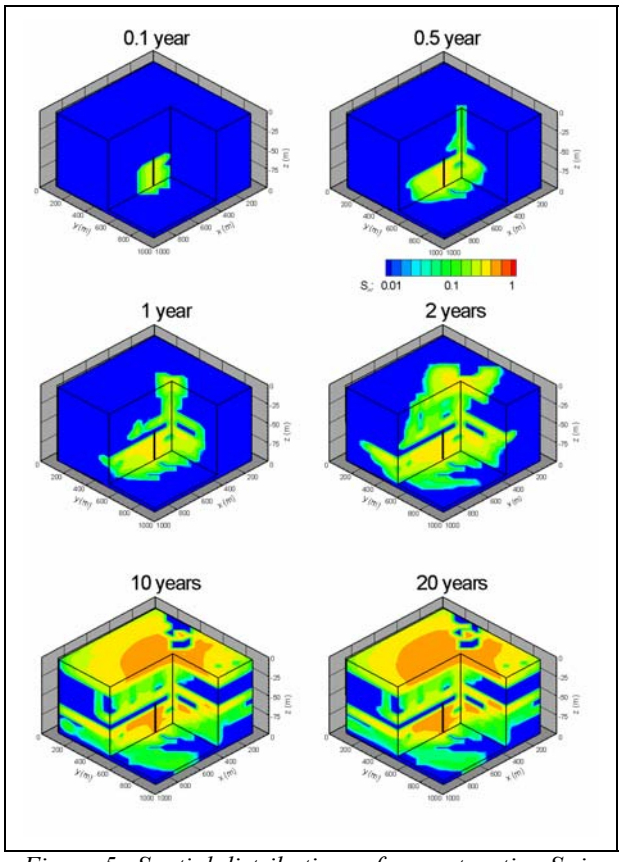

Figure 5. Spatial distributions of gas saturation S_g in basic Umbrella Point model during 20-year injection period

Figure 6 shows the analogous time sequence for a model with a finer vertical grid in which there are three grid layers for each depositional layer. The overall patterns of plume development are similar for the coarse and fine grids, but the fine-grid model shows higher concentrations of CO_2 as it allows resolution of buoyancy flow within individual sand channels.

Comparison of Figures 5 and 6 shows that after one year, the fine-grid model appears to contain more CO_2. To quantify CO_2 sequestration, we define the capacity factor C as the fraction of a specified volume of the subsurface containing CO_2. Capacity factor can be broken down by phase: $C = C_g + C_l$, where C_g is the fraction of the subsurface containing CO_2 in the gas-like phase and C_l is the fraction containing CO_2 dissolved in the aqueous phase. We have

$$C_g = \langle S_g \phi \rangle \quad (1)$$

$$C_l = \langle S_l X_l^{CO2} \rho_l / \rho_g \phi \rangle \quad (2)$$

where S_g and S_l are gas and liquid saturations,

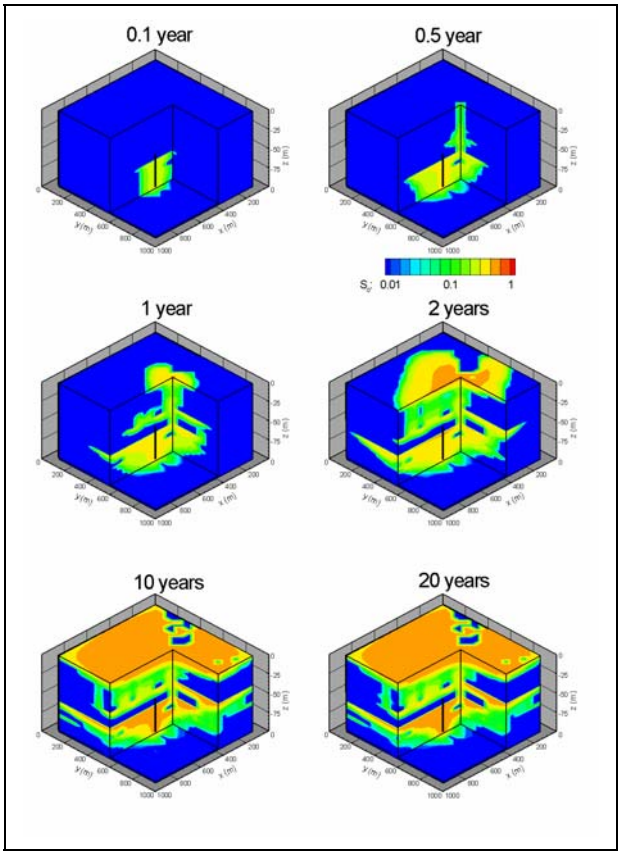

Figure 6. Spatial distributions of gas saturation S_g in fine-grid Umbrella Point model during 20-year injection period.

respectively, ϕ is porosity, X_l^{CO2} is the mass fraction of CO_2 dissolved in the aqueous phase, ρ_l and ρ_g are liquid- and gas-phase densities, respectively, and the angle brackets indicate an average over the specified volume. For the Umbrella Point model, the averaging volume is simply the model volume. For sequestration sites with no natural boundaries, defining the averaging volume may require careful deliberation to enable meaningful capacity comparisons to be made (Doughty et al., 2002).

Figure 7 shows C versus time for the basic and fine-grid models. Note that C increases linearly until the first CO_2 reaches the outer boundary of the model (the spill point) at about 2 years. Somewhat later, a quasi-steady state is reached in which the injection rate at the well nearly balances CO_2 flow out the lateral model boundaries. Figure 7 shows that significantly less CO_2 remains in the fine-grid model, where intra-sand channel buoyancy flow can be resolved and gas-like CO_2 becomes concentrated at the top of sand layers. Relative permeability effects then enable it to flow more readily to the open side boundaries of the model. Because the view of the model shown in Figures 5 and 6 is from above, the fine-grid model appears to contain more CO_2 when it actually contains less.

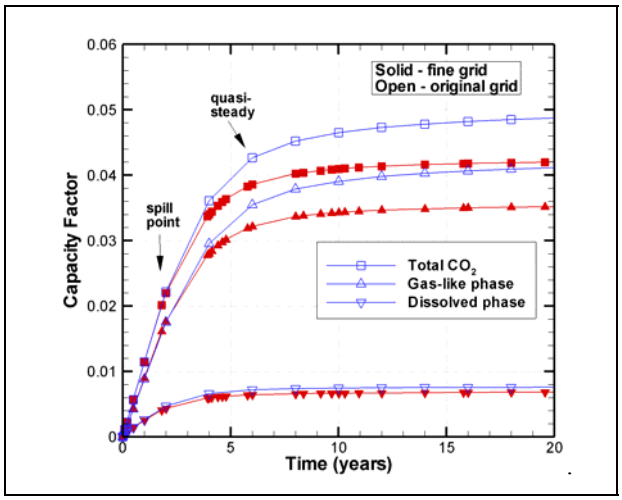

Figure 7. Capacity factor (fraction of subsurface containing CO_2) as a function of time during 20-year injection period.

South Liberty Pilot Site Model

CO_2 is injected at a rate of 250 metric tons per day (2.9 kg/s) for a period of 20 days, then the simulation continues with no injection for one year to watch the evolution of the CO_2 plume. Initial formation conditions are P = 150 bars, T = 64°C, and TDS = 100,000 ppm. Under these conditions, CO_2 has a density of 565 kg/m^3 and a viscosity of $4.3 \cdot 10^{-5}$ Pa·s. This injection schedule is comparable to what is planned for the pilot test, where the high costs of trucked-in CO_2 and field time must be balanced against the goal of injecting enough CO_2 to be able to monitor it in the subsurface. In particular, there will be one monitoring well located about 30 m updip of the injection well (labeled "SGH-4" and "new well", respectively, in Figure 4). One of the tasks of numerical modeling is to predict when injected CO_2 will arrive at the monitoring well.

Figure 8 shows gas-phase CO_2 plume development for the basic South Liberty model with a sequence of plan views of the top of the upward-coarsening sand, which is the top of the injection interval. During the 20-day injection period, the distribution of CO_2 is nearly radially symmetric around the injection well, but after injection ends, the buoyant flow of CO_2 updip becomes obvious. After one year, the bulk of the plume has moved updip of both the injection and monitoring wells. The irregular shape at the leading edge of the plume reflects flow around a shaley region (Figure 4).

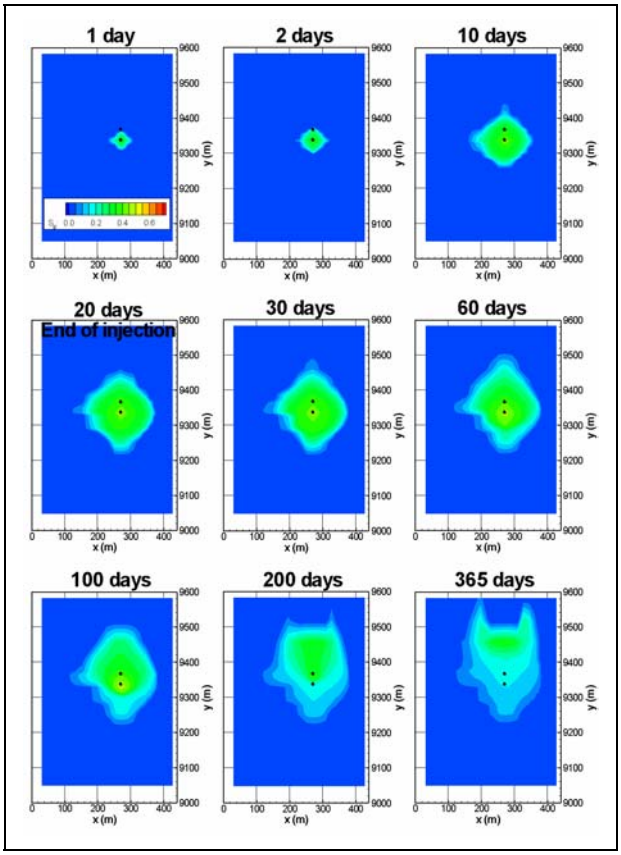

Figure 8. Time sequence of S_g distributions at top of upward-coarsening sand in South Liberty model, with five-point differencing, a non-uniform grid, and generic characteristic curves. Positive y-direction is updip; injection and monitoring wells are shown.

During the injection period, the plan view of the CO_2 plume actually looks more diamond-shaped than circular (Figure 8, top row). The model has homogeneous properties close to the injection well (Figure 4), so the lack of radial symmetry may be due to grid effects. To investigate the role of the grid, two alternative models were developed.

The diamond-shape of the early CO_2 plume is a hallmark of the preferential flow that typically arises along the axis directions in a rectangular grid that uses five-point differencing for lateral connections (i.e., four lateral connections for each grid block, one to each of its nearest neighbors). This problem can be ameliorated by using nine-point differencing for lateral connections (i.e., eight lateral connections for each grid block, the usual four nearest neighbors, plus the four nearest diagonal neighbors).

The implementation of nine-point differencing used here (K. Pruess, private communication, 1996) requires a laterally regular grid with square grid blocks. In the original grid, lateral spacing ranges from 2 m at the wells, to about 60 m near the closed edges of the model, to several hundred meters to the southwest, where the model extends far enough to act unbounded (Figure 4). A new grid with a uniform lateral spacing of 7.5 m was created. This grid will not resolve near-well behavior as well as the original grid and it has a constant-pressure boundary rather than extending far in the down-dip direction – a concession to size limitations of the computer being used for the simulations.

Figures 9 and 10 show plume development for the uniform grid with five-point and nine-point differencing for lateral connections, respectively. During the injection period, nine-point differencing produces a more circular plume, as expected. An unanticipated result is that during the post-injection period, the added lateral flow enabled by nine-point differencing slightly increases updip translation of the plume.

Comparison to the plume resulting from the non-uniform grid (Figure 8) makes it apparent that the preferential flow in the grid axis directions is exacerbated by the coarsening of the grid away from the wells, which further distorts the shape of the plume by enhancing spreading due to numerical dispersion. Spreading due to phase dispersion is an important aspect of plume evolution; it is undesirable to mask this process with spurious numerical effects. Moreover, with the more accurate plume depiction afforded by a finer grid, subtle irregularities in the plume shape may be attributed to geological features. In particular, the small indentations in the lower left quadrant of the plume, visible starting at 20 days, reflect gaps in the overlying thin shale layer, where CO_2 is leaking into the upper half of the model (see Figure 4).

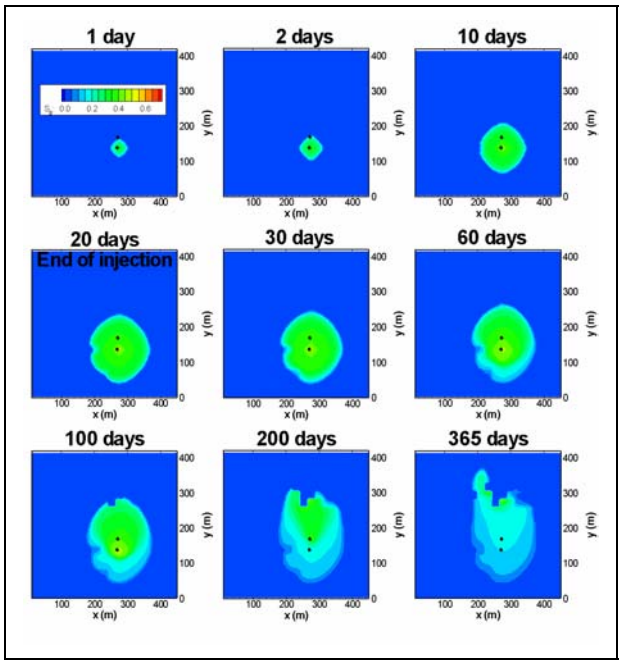

Figure 9. Time sequence of S_g distributions at top of upward-coarsening sand in South Liberty model with five-point differencing, a uniform grid, and generic characteristic curves.

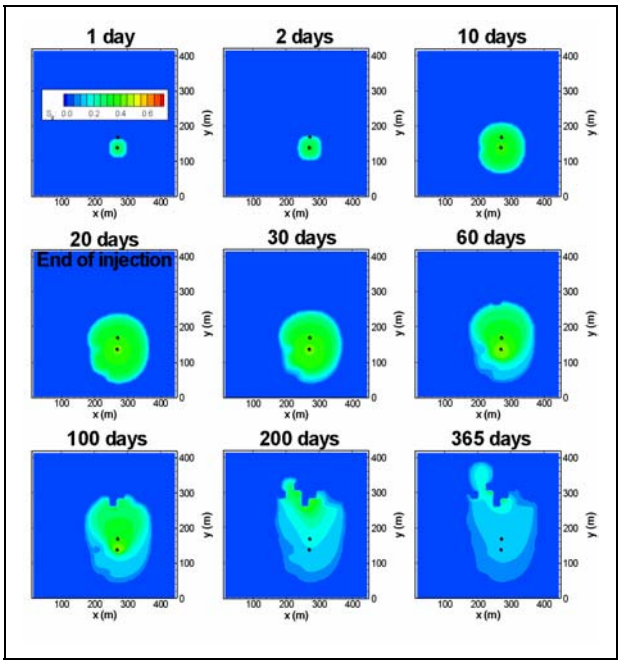

Figure 10. Time sequence of S_g distributions at top of upward-coarsening sand in South Liberty model with nine-point differencing, a uniform grid, and generic characteristic curves.

Recent studies (M. Holtz, private communication, 2002) have indicated that typical characteristic curves for the sand facies of the Frio formation in the vicinity of the South Liberty field have somewhat different features than the generic characteristic curves used thus far. Figure 11 compares generic and "Frio-like" relative permeability curves. The generic curves use the van Genuchten (1980) functional form for liquid relative permeability k_{rl} and the Corey (1954) functional form for gas relative permeability k_{rg} whereas the Frio-like curves use Corey curves for each. The more significant distinction between the two sets of curves is the residual saturations used (see Figure 11). The differences in residual saturation act to shift the Frio-like curves to the left. That is, over the entire range of saturation values, the Frio-like curves show greater liquid mobility and less gas mobility.

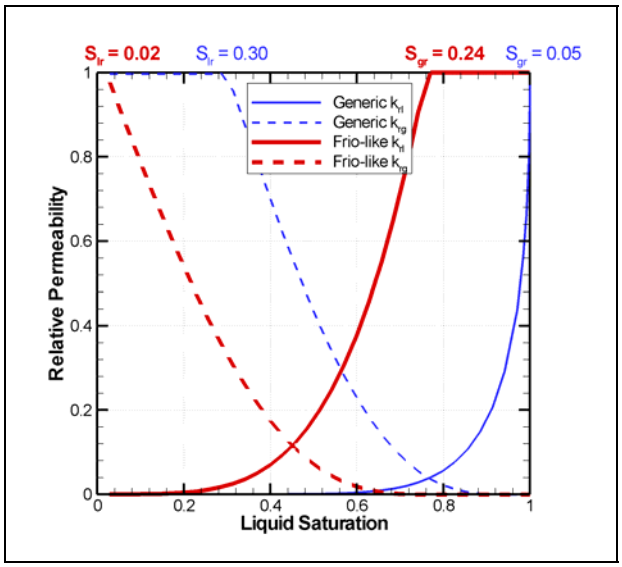

Figure 11. Relative permeability curves used for the South Liberty simulations.

Figure 12 shows plume development for the Frio-like characteristic curves. Compared to the case with generic characteristic curves (Figure 8), during the injection period, the gas-like CO_2 plume is much more compact (higher gas saturation and smaller radial extent). After injection ends, the plume begins to spread, and it does not take long for the gas saturation to decrease to the residual value, making the plume essentially immobile. Thus, the plume does not migrate nearly as far updip as for the generic characteristic curves, but remains localized near the injection well.

The differences in plume behavior for the different sets of characteristic curves have important ramifications for the pilot test. Choices about the timing, location, and sensitivity of monitoring techniques depend strongly on the nature of the CO_2 plume. For example, although the arrival time of the plume at the monitoring well does not depend too much on the choice of residual saturations (2-3 days in either case), the passage of the trailing edge certainly does. A series of geophysical surveys designed to image plume passage could be completed over the course of one year for the generic characteristic curves, but for the Frio-like characteristic curves the same series would show an essentially steady plume.

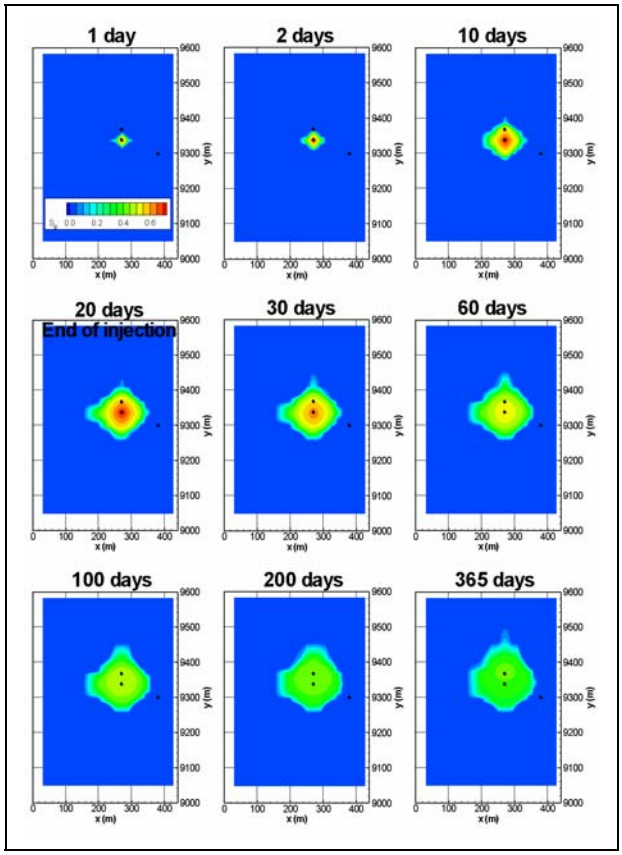

Figure 12. Time sequence of S_g distributions at top of upward-coarsening sand in South Liberty model with five-point differencing, a non-uniform grid, and Frio-like characteristic curves.

CONCLUSIONS

Modeling the injection and storage of supercritical CO_2 in brine-bearing formations has provided valuable insights into flow and transport behavior. Subtle interplays between physical and numerical effects can occur, requiring that model development choices be made with care. In particular, grid resolution and orientation effects can produce results that mimic and mask physical processes accompanying buoyant flow in heterogeneous systems.

The present study has reiterated the well-known finding that the choice of characteristic curves is very important. A key issue regarding the feasibility of geologic sequestration in general is whether there is adequate capacity in the subsurface to store the extremely large quantities of CO_2 necessary to impact the global carbon balance. The typical gas saturation in the CO_2 plumes (i.e., the "concentration" of CO_2) varies by nearly a factor of two for the different characteristic curves – a significant effect. Moreover, with high residual gas saturation, sites that are not perfectly sealed become viable for sequestration, as moderate saturation decreases arising from phase dispersion cause the plume to become immobile.

ACKNOWLEDGMENT

We thank Victor Malkovsky of IGEM, Moscow, Russia for kindly providing us with his computer programs of the CO_2 property correlations of V. V. Altunin; Christopher Green, now of U.S.G.S Menlo Park, for generating the TproGS property distributions; and Paul Knox of Texas Bureau of Economic Geology for providing the idealized representations of the Frio formation. We are also grateful to Stefan Finsterle and Curt Oldenburg of Lawrence Berkeley National Laboratory for their technical reviews. This work is supported by the Assistant Secretary for Fossil Energy, Office of Coal and Power Systems through the National Energy Technology Laboratory, and by Lawrence Berkeley National Laboratory under Department of Energy Contract No. DE-AC03-76SF00098.

REFERENCES

Altunin, V.V., *Thermophysical properties of carbon dioxide* (in Russian), Publishing House of Standards, Moscow, 1975.

Battistelli, A., C. Calore, and K. Pruess, The simulator TOUGH2/EWASG for modeling geothermal reservoirs with brines and non-condensible gas, *Geothermics,* 26(4), 437-464, 1997.

Carle, S.F. and G.E. Fogg, Transition probability based indicator geostatistics, *Mathematical Geology,* 28(4), 453-477, 1996.

Carle, S.F. and G.E. Fogg, Modeling spatial variability with one and multidimensional continuous-lag Markov chains, *Mathematical Geology*, 29(7), 891-917, 1997.

Corey, A.T., The interrelation between gas and oil relative permeabilities, *Producers Monthly*, 38-41, November 1954.

Doughty, C., K. Pruess, S.M. Benson, S.D. Hovorka, P.R. Knox, and C.T. Green, Capacity Investigation of Brine-Bearing Sands of the Frio Formation for Geologic Sequestration of CO_2, First National Conference on Carbon Sequestration, May 14-17, Washington DC, National Energy Technology Laboratory, 2001.

Doughty, C., S.M. Benson, and K. Pruess, Capacity investigations of brine-bearing sands for geologic sequestration of CO_2, GHGT-6 Conference, Kyoto, Japan, September 30 – October 4, 2002.

Fogg, G.E., S.F. Carle, and C.T. Green, A connected network paradigm for the alluvial aquifer system, in D. Zhang and C.L Winter, eds., Theory, modeling, and field investigation in hydrogeology: a special volume in honor of Shlomo P. Neuman's 60th birthday, Geol. Soc. of Am., Special Paper 348, 2001.

Galloway, W.E., *Depositional architecture of Cenozoic gulf coastal plain fluvial systems*, Circular 82-5, University of Texas at Austin, Bureau of Economic Geology, 1982.

Hovorka, S.D., C. Doughty, P.R. Knox, C.T. Green, K. Pruess, and S.M. Benson, Evaluation of brine-bearing sands of the Frio formation, upper Texas gulf coast for geological sequestration of CO_2, First National Conference on Carbon Sequestration, May 14-17, Washington DC, National Energy Technology Laboratory, 2001.

Knox, P.R., C. Doughty, and S.D. Hovorka, Impacts of buoyancy and pressure gradient on field-scale geological sequestration of CO_2 in saline aquifers, AAPG Annual Meeting, Salt Lake City, May, 2003.

Pruess, K. and J. Garcia, Multiphase flow dynamics during CO2 disposal into saline aquifers, *Environmental Geology*, 42, 282-295, 2002.

Pruess, K., C. Oldenburg, and G. Moridis, *TOUGH2 User's Guide, Version 2.0*, Report LBNL-43134, Lawrence Berkeley National Laboratory, Berkeley, Calif., 1999.

Pruess, K., T. Xu, J. Apps, and J. Garcia, Numerical modeling of aquifer disposal of CO_2 (SPE 83695), *SPE Journal*, 49-60, March 2003.

van der Meer, L.G.H., The CO_2 storage efficiency of aquifers, *Energy Conservation and Management*, 36(6-9), 513-518, 1995.

van Genuchten, M.Th., A closed-form equation for predicting the hydraulic conductivity of unsaturated soils, *Soil Sci. Soc. Am. J.*, 44, 892-898, 1980.

Vining, M.R., Reserve growth in a mixed sequence of deltaic and barrier-island Frio sandstones, Umbrella Point field, Chambers County, Texas, *Gulf Coast Assoc. of Geol. Soc. Trans.*, 47, 611-619, 1997.